J Nanopart Res (2018) 20: 157
https://doi.org/10.1007/s11051-018-4260-0

RESEARCH PAPER

Synthesis, characterization, and thermal stability of SiO_2/TiO_2/CR-Ag multilayered nanostructures

Gabriela Díaz · Yao-Jen Chang · Ara Philipossian

Received: 10 April 2018 / Accepted: 23 May 2018 / Published online: 3 June 2018

Abstract The controllable synthesis and characterization of novel thermally stable silver-based particles are described. The experimental approach involves the design of thermally stable nanostructures by the deposition of an interfacial thick, active titania layer between the primary substrate (SiO_2 particles) and the metal nanoparticles (Ag NPs), as well as the doping of Ag nanoparticles with an organic molecule (Congo Red, CR). The nanostructured particles were composed of a 330-nm silica core capped by a granular titania layer (10 to 13 nm in thickness), along with monodisperse 5 to 30 nm CR-Ag NPs deposited on top. The titania-coated support (SiO_2/TiO_2 particles) was shown to be chemically and thermally stable and promoted the nucleation and anchoring of CR-Ag NPs, which prevented the sintering of CR-Ag NPs when the structure was exposed to high temperatures. The thermal stability of the silver composites was examined by scanning electron microscopy (SEM) and high-resolution transmission electron microscopy (HRTEM). Larger than 10 nm CR-Ag NPs were thermally stable up to 300 °C. Such temperature was high enough to destabilize the CR-Ag NPs due to the melting point of the CR. On the other hand, smaller than 10 nm Ag NPs were stable at temperatures up to 500 °C because of the strong metal-metal oxide binding energy. Energy dispersion X-ray spectroscopy (EDS) was carried out to qualitatively analyze the chemical stability of the structure at different temperatures which confirmed the stability of the structure and the existence of silver NPs at temperatures up to 500 °C.

Keywords Ag nanoparticles · Nanostructures · Thermal stability · Electron microscopy · Sintering · Nanocomposites

G. Díaz (✉) · A. Philipossian
Department of Chemical and Environmental Engineering, University of Arizona, Tucson, AZ 85721, USA
e-mail: gdiaz10@email.arizona.edu

Y.-J. Chang
Imaging Cores – Materials Imaging and Characterization Facilities, University of Arizona, Tucson, AZ 85721, USA

Introduction

The development of nanoscale particles continues to receive tremendous interest from both academic and industrial circles. Fields involving biosensors (Andrade et al. 2010; Wang et al. 2012; Pham et al. 2017), optical devices (Lee et al. 2006; Ye et al. 2015), catalysts (Shter et al. 2007; Maldonado et al. 2010; Zhou et al. 2011; Aouat et al. 2013; Dong et al. 2015), and integrated circuits (Su et al. 2016), among others, have shown improvements to the practical applications by using noble metal nanoparticles (NPs) with tunable structures and properties. The main interest in metal NPs is on their distinct physical, chemical, and biological properties compared with their isolated molecules and bulk counterparts (Luo et al. 2008; Cao et al. 2010; Abou El-Nour et al. 2010; Volkman et al. 2011; Su et al. 2016). Metal nanoparticles have demonstrated enhanced reactivity

and selectivity in different chemical processes because of the abundant fraction of atoms on their surface which behave as catalytic active centers. Silver nanoparticle-based catalysts have proven high catalytic activity and selectivity for producing numerous organic compounds, such as formaldehyde, ethylene oxides, epoxides, and aldehydes (Shter et al. 2007; Abou El-Nour et al. 2010; Cao et al. 2010; Maldonado et al. 2010; Chen et al. 2011; Aouat et al. 2013; Dong et al. 2015; Zhang et al. 2015). However, direct large-scale industrial use of silver NPs has been drastically hampered by their lack of thermal and chemical stability (Yan et al. 2005; Luo et al. 2008; Cao et al. 2010). It is well documented that temperature is one of the principal parameters that affect the performance of these materials (Luo et al. 2008; Safaei and Attarian Shandiz 2009; Cao et al. 2010; Volkman et al. 2011) as the exposure of metal NPs to significantly high temperatures leads to the dissociation, diffusion, aggregation, and coalescence of their surface atoms or entire particles (Moon et al. 2005; Volkman et al. 2011; Aouat et al. 2013; Hansen et al. 2014). Particle growth is the direct outcome of such processes.

The metal NP growth or sintering takes place via 2 operational mechanisms, namely, atomic migration or Ostwald ripening (OR) and particle migration and coalescence (PMC). Ostwald ripening involves the detachment of metal atoms, followed by their migration (driven by differences in free energies) and final attachment to larger particles. Particle migration and coalescence occur via diffusion of entire particles along the support surface, followed by collision and coalescence when particles approach one another (Moulijn et al. 2001; Volkman et al. 2011; Fang and Wang 2013; Hansen et al. 2014). Recent studies have shown that sintering can be examined by the direct observation of particle morphologies, sizes, and polycrystallinity (Volkman et al. 2011). Sintering takes place at temperatures greater than 500 °C for conventional microparticles, but for metal NPs, it can occur at much lower temperatures such as 150 °C (Moon et al. 2005). This abrupt drop in temperature is attributed to the large surface area to volume ratio of the NPs which can alter their thermodynamic properties (Luo et al. 2008; Safaei and Attarian Shandiz 2009; Ahmed et al. 2010; Cao et al. 2010; Verma et al. 2014; Argyle and Bartholomew 2015; Kopangkhotso et al. 2015).

Smart combinations of different nanostructured materials with specific structures have been developed to efficiently stabilize nanomaterials. Such complex nanostructures have shown multiple functionalities for a variety of applications which are difficult to achieve with single-component particles (Wang et al. 2012). Yet, to minimize sintering effects, metal NPs have been deposited on different supports (Yan et al. 2005; Maldonado et al. 2010; Zhang et al. 2015), doped with polymers (Shter et al. 2007; Yosef and Avnir 2011; Aouat et al. 2013; Dai et al. 2018), coated with thermally stable materials (Hanprasopwattana et al. 1996; Henglein and Giersig 1999; Lee et al. 2006; Ye et al. 2015), alloyed with other metals (Pham et al. 2017), and integrated with mesoporous structures (Alford et al. 2003). Cao et al. (2010) compiled the approaches that have been explored to prevent the sintering of metal NPs and categorized them in three groups as follows: (1) modification of the metal-support interface through the construction of interfacial structures, (2) modification of the metal nanoparticle's elemental composition, and (3) modification of the support via proper nanostructuring.

In this study, we describe the preparation, characterization, and thermal stability of SiO_2/TiO_2/CR-Ag multilayered nanostructures. Our general methodology combines all three previously mentioned stabilization approaches. The proposed structure has a core support consisting of silica particles (SiO_2) coated by a thick layer of titanium dioxide (TiO_2) creating surface defects. Such thermally stable defects have proven to be active nucleation sites (Hanprasopwattana et al. 1996; Wallace et al. 2005; Yan et al. 2005) which allow for subsequent deposition and dispersion of silver NPs. We then dope silver metal ions with Congo Red (CR) organic molecules (Shter et al. 2007; Yosef and Avnir 2011; Aouat et al. 2013) and deposit them on the TiO_2 layer. Both TiO_2 surface defects and CR doping have been previously shown to change the thermodynamic and catalytic properties of silver NPs separately (Yan et al. 2005; Aouat et al. 2013; Dong et al. 2015). The interactions between the support (TiO_2 layer in our case) and the active metal nanoparticles are not entirely understood, but it is known that the nature of the support changes the catalytic activity and the stability of metal NPs (Yan et al. 2005; Cao et al. 2010; Zhang et al. 2015). On the other hand, CR is abundant in functional groups which can effectively increase the specific area of the doped metal NPs and therefore their absorption capacity and catalytic applications; also CR is inexpensive and easily available (Shter et al. 2007; Aouat et al. 2013; Dai et al. 2018).

Our paper demonstrates that the combination of both methodologies results in thermally stable silver-based

structures that are capable of tolerating temperatures as high as 500 °C. It is highly desirable to explore the feasibility of our design to other metal nanoparticles (Pt, Ru, Cu, Au) that have proved high catalytic activity and poor thermal stability. In this study, we have directly followed the CR-Ag NP morphology, size, and crystallinity using a battery of techniques including scanning electron microscopy (SEM), transmission electron microscopy (TEM), UV-Vis spectroscopy, and elemental mapping (EDS). This operational investigation could be helpful for the design of thermally and chemically stable heterogeneous catalysts.

Experimental details

Materials

The following substances were used in this study: tetraethylorthosilicate (TEOS, 99%), ammonium hydroxide (NH_4OH), A.C.S. grade ethanol, titanium (IV) butoxide (TBOT), silver nitrate ($AgNO_3$), Congo Red ($C_{32}H_{22}N_6Na_2O_6S_2$), trisodium citrate ($Na_3C_6H_5O_7$), and sodium hypophosphite ($NaPO_2H_2$). All chemicals employed for the synthesis work were as-received (Sigma-Aldrich) as no further purifications were made. Milli-Q purified water was utilized for all aqueous solutions.

Synthesis of SiO_2 particles

In general, we followed an approach similar to those described elsewhere (Stöber et al. 1968; Costa et al. 2003). In our case, the following methodology was utilized to synthesize silica particles having an average nominal diameter of 330 nm by the sol-gel process. A 15 *v*/*v*% TEOS solution in ethanol was prepared and kept under stirring. In parallel, a mixture of 21 *v*/*v*% DI water, 12 *v*/*v*% ammonium hydroxide, and ethanol was prepared and stirred for 1 min; then, the second solution was poured into the first one (14:11, vol.) under constant stirring for 2 h. The final dispersion was rinsed three times with DI water by centrifugation-ultrasonic dispersion. Warm DI water (50 °C) was used to eliminate any organic residues. Lastly, the particles were dispersed in 5 to 10 mL of ethanol, dried overnight at 80 °C, and stored for later use.

Deposition of TiO_2 layer—SiO_2/TiO_2 particles

Examples of depositing TiO_2 coatings can be found elsewhere (Hanprasopwattana et al. 1996; Ye et al. 2015; Chen et al. 2016). In our case, we used 0.6 g of SiO_2 particles and dispersed them in 100 mL of ethanol followed by sonication for 30 min. After sonication, 150 mL of 2.6 *v*/*v*% TBOT solution in ethanol was added dropwise to the above solution and sonicated for 15 min. Then, 100 mL of DI water was added under vigorous stirring. The refluxed reaction occurred at 80 °C for 90 min. The resulting SiO_2/TiO_2 particles were purified by centrifugation, redispersed in ethanol, dried overnight at 80 °C, and calcinated at 650 °C in N_2 for 4 h.

Synthesis of CR-Ag nanoparticles—SiO_2/TiO_2/CR-Ag nanostructures

Members of the Avnir research group (Shter et al. 2007; Yosef and Avnir 2011; Aouat et al. 2013) have introduced a method for the entrapment of organic molecules in a metallic silver matrix. Such new family of hybrid materials has proven to possess superior catalytic activity (Yosef and Avnir 2011), the practicality of which motivated us to adopt parts of their method to synthesize a new thermally stable composite. In our current approach, the synthesis and stabilization of metal silver ions (Ag^+) were achieved by the reduction of $AgNO_3$ with two reducing and stabilizing agents, namely sodium citrate (Henglein and Giersig 1999) and sodium hypophosphite (Yosef and Avnir 2011). We first dispersed 0.02 g of SiO_2/TiO_2 particles in 15 mL of water by sonication. In parallel, two solutions were prepared (a 2.35 mM $AgNO_3$ solution and a 0.17 mM of Congo Red) and stirred for 5 min each. The two solutions were mixed (75 and 10 mL, respectively) to form a third one which was sonicated for 30 min. Then, the SiO_2/TiO_2 aqueous suspension was added to the third solution and incubated under vigorous stirring for 2 h at room temperature. Following this step, 0.015 g of sodium citrate and 0.022 g of sodium hypophosphite were added to the suspension. The final pH-neutral solution was stirred for 110 min at 80 °C. The precipitate was washed three times with water by centrifugation-ultrasonic dispersion until the supernatant became clear. Finally, the precipitate was redispersed in 5 mL of EtOH and dried at 100 °C overnight. For the sake of consistency, a large

batch of SiO_2/TiO_2/CR-Ag particles was prepared and used for all the experiments and analyses in our study.

Analysis and material characterization

SEM was carried out on a Hitachi S-4800 HR field emission SEM equipped with energy-dispersive X-ray microanalysis. TEM analysis was carried out on a Hitachi HF-5000 equipped with a probe aberration corrector for high-resolution (78 pm) scanning TEM (STEM) imaging; an Oxford Instruments large solid angle (2.0 sr) energy-dispersive X-ray spectrometer for chemical mapping, and a Gatan GIF Quantum ER EELS spectrometer (with dual EELS capability) for atomic-scale chemical spectroscopy and imaging. TEM image detectors include bright-field STEM, annular (both medium and high angle) dark field, and secondary electron. For SEM and TEM analysis, a few micrograms of the resulting powder were dispersed in water by ultrasonication and drop-casted on commercially available copper grids (SEM) and lacey carbon-coated copper grids (TEM). UV-visible absorption spectroscopy measurements were performed on a ThermoScientific Genesys 10S UV-Vis system. The thermal treatment was carried out in argon, at a flow rate of 150 SCCM, in an automated hot-wall, quartz-lined annealing furnace equipped with three thermocouples which ensured minimal (i.e. < 1 °C) variation in temperature. All annealing processes lasted for 1 h at the specified temperature with ramp up and ramp down rates both at 5 °C/min.

Results and discussion

Multilayered SiO_2/TiO_2/CR-Ag nanostructures

SEM images of pure SiO_2 particles show spherical structures with smooth surfaces and free of organic residues. Additionally, there was no observable necking between adjacent particles (Fig. 1a, b). Also, as shown in Fig. 1c, the SiO_2 spheres have a wide range of sizes with a nominal average diameter of 330 nm. We had originally believed that the wide SiO_2 particle size distribution might affect the subsequent deposition of a uniform TiO_2 film; however, for the most part, we can see in Fig. 2a, b that the TiO_2 layer turned out to be reasonably regular in thickness (approx. 10 to 13 nm) with no apparent agglomeration of the core SiO_2 particles. The sequential hydrolysis reactions allowed the TiO_2 deposition on the SiO_2 surface with no need of an "additional" ligand molecule. Figure 2b also shows the presence of a secondary phase of titania in the form of branched segments protruding away from the silica particles. The calcination step after TiO_2 deposition is crucial in forming a granular TiO_2 film on the surface of the silica spheres (Fig. 2a). Such superficial features are advantageous due to their inherently large density of dangling bonds, which is determined by the roughness and curvature of the surface allowing greater CR-Ag deposition. During the calcination process, temperature promotes the loss of OH groups and the subsequent crystallization of TiO_2 by the rearrangement of the Ti-O network (Yu et al. 2003; Ye et al. 2015). For comparison, Fig. 2c shows silica spheres coated with TiO_2 before the subsequent calcination step; an amorphous TiO_2 layer coating the surface of the SiO_2 spheres can be observed. The calcination process was carried out at 650 °C to ensure the thermal stability of the TiO_2 film during the thermal treatment (200 to 500 °C) since any rearrange in the atomic structure of the TiO_2 layer can trigger the sintering of the CR-Ag NPs deposited on its surface.

The Avnir research group (Shter et al. 2007; Yosef and Avnir 2011; Aouat et al. 2013) has demonstrated the entrapment of the organic molecule, Congo Red, within metals, where monodisperse CR-Ag clusters have been accomplished by adjusting the pH and the reaction time of their proposed synthesis methods. In our study, the reaction time was reduced to 110 min without any pH adjustment. Figure 3 shows SEM images of the multilayered structures after CR-Ag deposition (SiO_2/TiO_2/CR-Ag nanostructures). The action of the two reducing-stabilizing agents avoided the agglomeration of CR-Ag NPs during their nucleation and growth resulting in a well-distributed CR-Ag NPs deposited on the TiO_2 surface. Figure 3a shows fully coated SiO_2/TiO_2 spheres by CR-Ag NPs, with no visible signs of the underlying TiO_2 layer. We should also note the wide size distribution of the CR-Ag NPs (approx. 5 to 30 nm) which turned out to be advantageous because we could closely monitor the effect of temperature on NPs with different diameters. Figure 3b shows that there is no agglomeration between SiO_2/TiO_2/CR-Ag particles and confirms the presence of CR-Ag NPs evenly coating all the surfaces including the titania second phase.

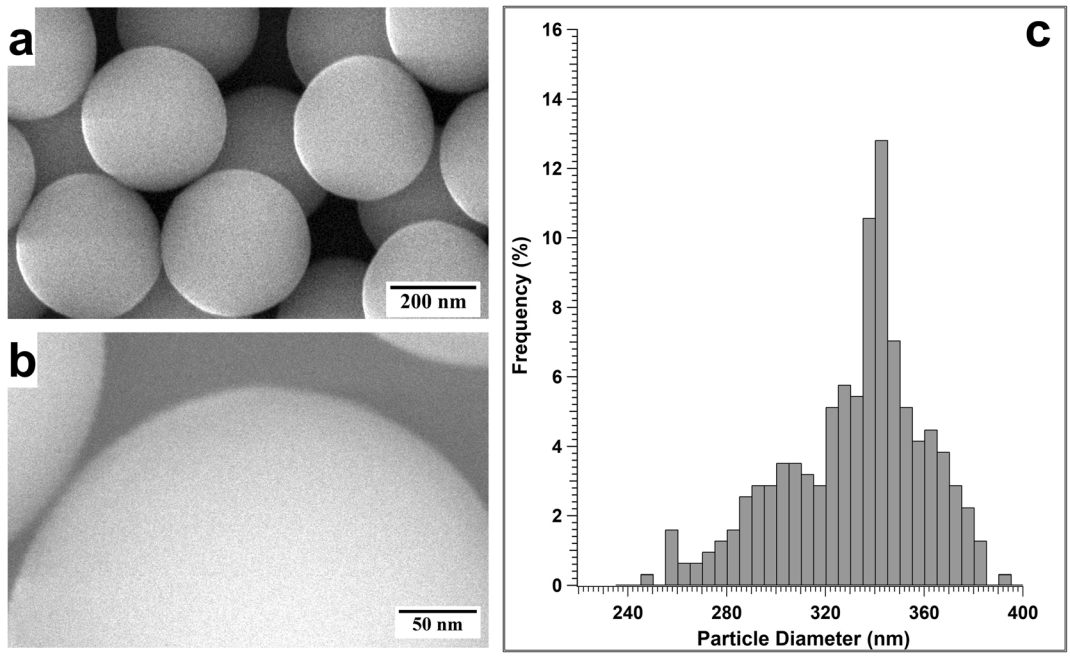

Fig. 1 SiO_2 spheres: **a** SEM 200 nm and **b** SEM 50 nm. **c** Particle size distribution

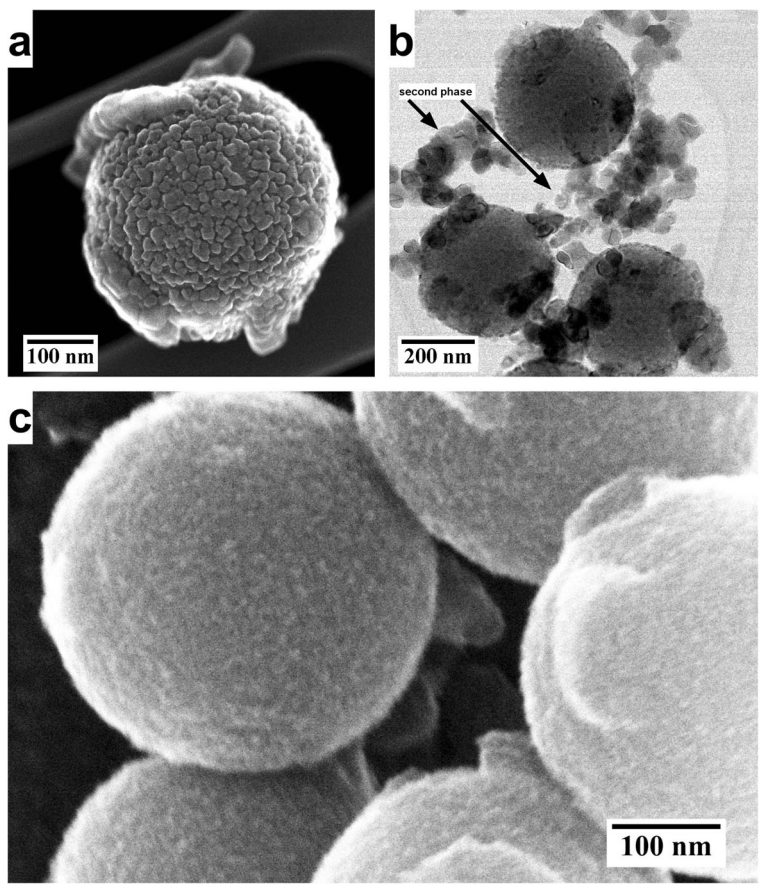

Fig. 2 SiO_2/TiO_2 structures. **a** SE, crystalline TiO_2 layer—650 °C calcination; **b** bright field, formation of TiO_2 second phase; and **c** SEM, SiO_2/TiO_2 structures before calcination step

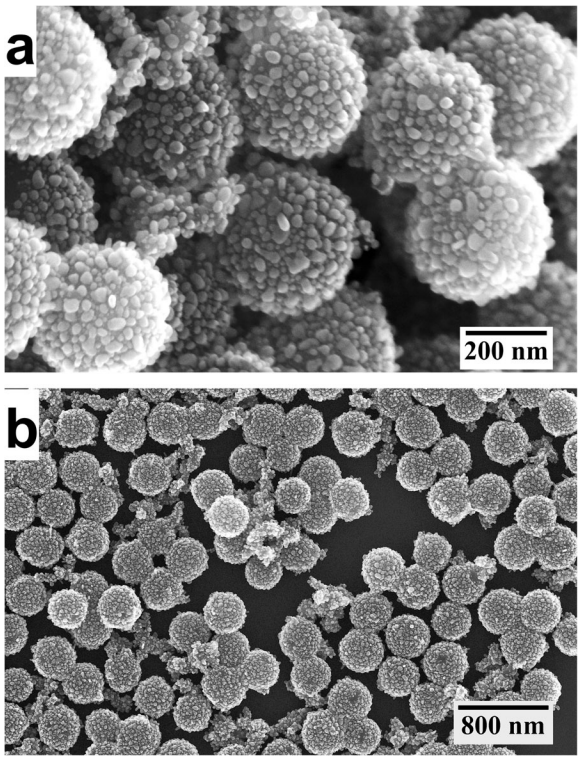

Fig. 3 SEM SiO_2/TiO_2/CR-Ag composites. **a** Wide size distribution of CR-Ag clusters. **b** Highly dispersed SiO_2/TiO_2/CR-Ag structures

Thermal stability of SiO_2/TiO_2/CR-Ag nanostructures

Drying, performed overnight at 100 °C, was the final step in preparing the SiO_2/TiO_2/CR-Ag particles. In our study, dried SiO_2/TiO_2/CR-Ag nanostructures, without subsequent annealing, were considered as the control sample against which all other structures were compared. Morphology, crystallinity, and size of the CR-Ag NPs were monitored after annealing at 200, 300, and 500 °C.

First, the effects of temperature on the multilayered SiO_2/TiO_2/CR-Ag particles were analyzed by UV-Vis. The corresponding UV-Vis spectra of the SiO_2/TiO_2/CR-Ag composites before and after thermal treatment, as well as before and after CR-Ag deposition, are shown in Fig. 4. SiO_2 spheres (a) show no characteristic peaks in the UV-Vis spectra because SiO_2 particles do not absorb photons in the visible portion of the spectrum. On the other hand, SiO_2/TiO_2 structures (b) generate an intense absorption peak around 330 to 370 nm which corresponds to the excitation of electrons from the valence to the conduction band of TiO_2. For the SiO_2/TiO_2/CR-Ag particles with no heating (c), two broad absorption peaks can be seen: one is centered at approx. 300 and the other at approx. 418 nm. This stems from strong scattering caused by different silver species. The broad absorption band at 418 nm is the characteristic absorbance of metallic silver NPs with wide-ranging diameters. The presence of the absorption band at 300 nm can be attributed to small ionic CR-Ag clusters which, on average, have an absorption band of 280 to 330 nm (Chen et al. 2011; Al-Thabaiti et al. 2016). At an exposure temperature of 200 °C (d), the position of the absorption peaks remains the same indicating that the size distribution of silver NPs has not changed. However, the intensity increases which could indicate the aggregation of the ionic CR-Ag clusters. For the SiO_2/TiO_2/CR-Ag particles exposed to 300 °C (e), the band corresponding to silver metal species (at 418 nm) is slightly shifted to the left (i.e., a blue shift). For metal nanoparticles, the oscillation wavelength depends on several factors such as particle size and shape, and the nature of the surrounding medium among others. In this case, the observed changes in the absorbance curve can be related to size effects because of the applied temperature. The sample annealed at 500 °C (f) exhibits a wide peak which could suggest the low abundance, and the polydispersity, of silver crystals. The peak at 300 nm fades out indicating the disappearance of the ionic species.

Next, TEM and high-resolution transmission electron microscopy (HRTEM) imaging were carried out to investigate the morphology and the particle size distribution of silver NPs at different annealing temperatures. It must be noted that the secondary electron (SE) detector is able to produce a representative 2D image of the area being examined. Coupled with this, the HRTEM allows for direct imaging of the atomic planes in the structure. As such, both detectors were used to investigate the thermal stability of Ag NPs. Qualitative EDS was also performed to display the presence and the spatial distribution of Ag species in each sample. To ensure that the whole structure was thermally stable, elemental Si, Ti, O, and C were also scanned for at all temperatures.

The SE image, alongside the HRTEM image and the elemental mapping (EDS) of SiO_2/TiO_2/CR-Ag structures with no annealing treatment, is shown in Fig. 5. Even though CR-Ag NPs have a wide range of sizes (4 to 30 nm) and there exist a wide variety of morphologies, Fig. 5a shows that CR-Ag NPs are homogeneously distributed on the irregular TiO_2 surface. In Fig. 5b, a stacking fault twin boundary (as a light gray band just to the right of the white arrow) can be observed which suggests

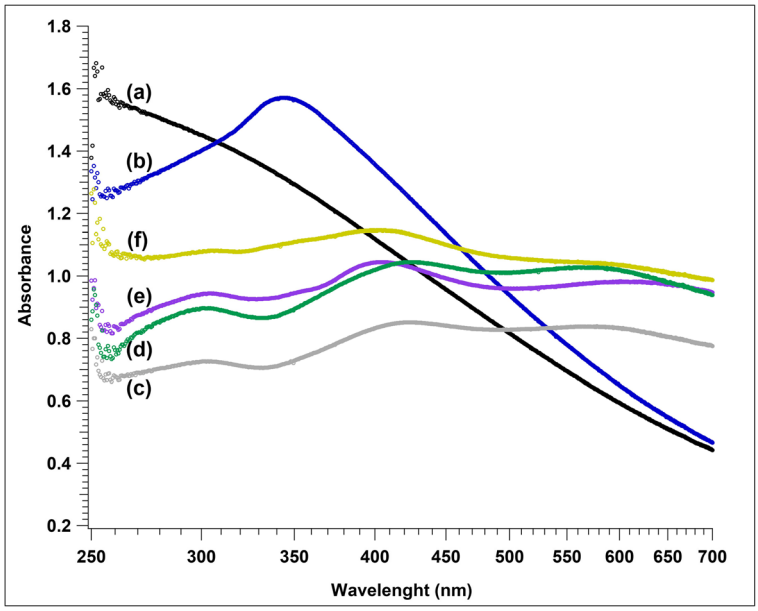

Fig. 4 UV-Vis spectra for **a** SiO_2 spheres, **b** SiO_2/TiO_2 structures, SiO_2/TiO_2/CR-Ag nanostructures at **c** 100 °C, **d** 200 °C, **e** 300 °C, and **f** 500 °C

the coexistence of two crystalline structures with arbitrary orientations which likely grew together. In its bulk form, Ag exhibits a cubic crystal structure with an FCC unit cell. However, the existence of hexagonal 4H-Ag phase

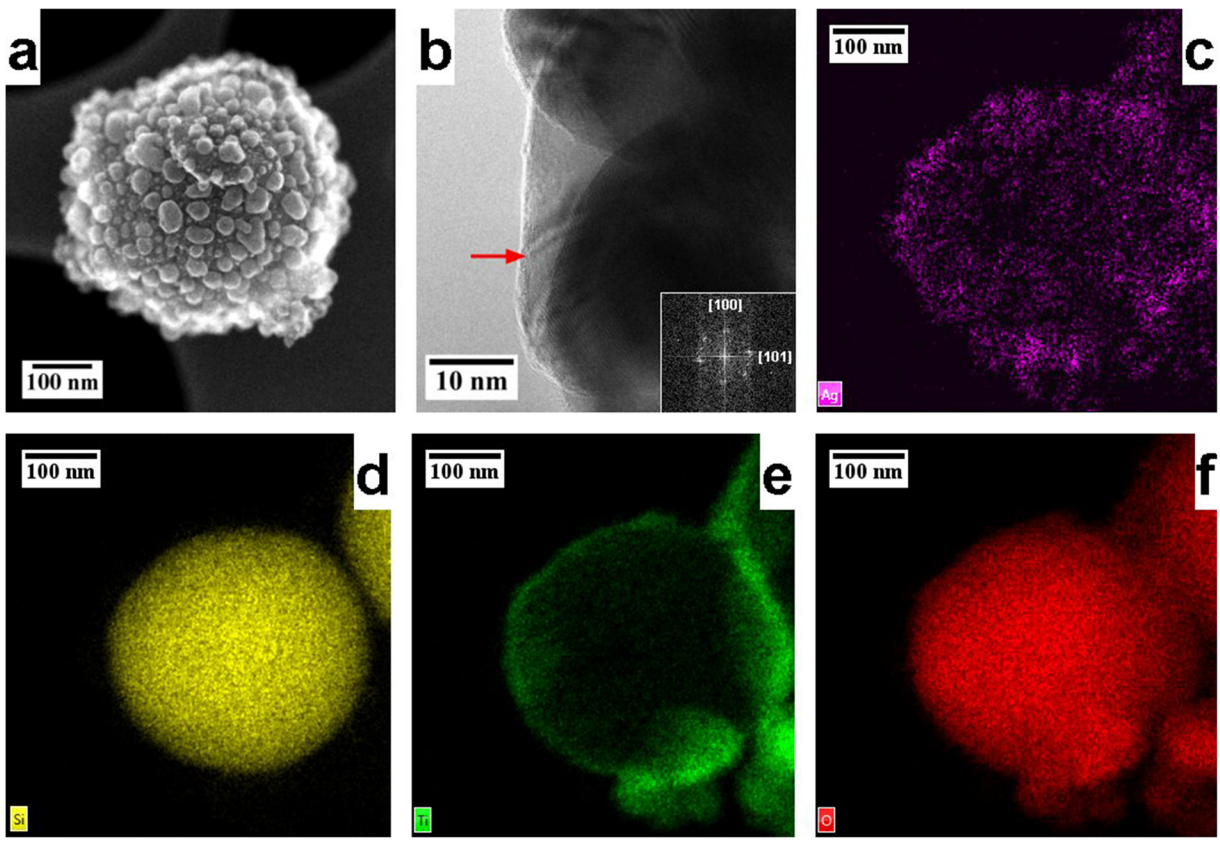

Fig. 5 SiO_2/TiO_2/CR-Ag nanostructures without heat treatment obtained via **a** SE and **b** HRTEM. EDS mapping for **c** Ag, **d** Si, **e** Ti, and **f** O

has been demonstrated for silver nanostructures (Chakraborty et al. 2011). The sample under study shows interplanar distance characteristics of hexagonal 4H-Ag crystal arrangements. To obtain the d-spacing, fast Fourier transformation of electron diffraction was utilized to generate the FFT diffractogram pattern (inset in Fig. 5b). Accordingly, interplanar distances of 2.58 and 2.44 Å corresponding to (100) and (101) Miller indices were measured for SiO_2/TiO_2/CR-Ag nanostructures that were not annealed. EDS mapping (Fig. 5c) corroborated the presence of well-distributed Ag metal species along the scanned particle. From the EDS spectra, we have confirmed the presence of oxygen species overlapping the areas occupied by Si and Ti which corroborates the chemical composition of SiO_2 and TiO_2 supports (Fig. 5d–f).

After SiO_2/TiO_2/CR-Ag particles were exposed to 200 °C, no changes were observed in the size of the CR-Ag NPs (Fig. 6a). However, a closer look at the sample allowed us to appreciate many Ag NPs ranging in size from 4 to 10 nm that were decorating the TiO_2 layer and the surface of larger silver crystals. The presence of such small particles on the surface of larger ones may have been due to the aggregation of ionic Ag clusters into fine particles at the higher temperature. Such discrete Ag NPs would have had high enough surface free energies to migrate and coalesce with the larger ones and become stable. On the other hand, Avnir and coworkers (Shter et al. 2007; Yosef and Avnir 2011; Aouat et al. 2013) have suggested that such small particles were due to the leakage of CR triggered by the high energy of the electron beam heating the Ag crystals. In Fig. 6b, fringes in the silver crystal can be seen. At 200 °C, the interplanar spacing is reduced to 2.36 Å which suggests a Miller index of (110) on the hexagonal 4H-Ag phase. EDS mapping shows the presence of a well-defined coating of silver NPs over the entire surface of SiO_2/TiO_2 structures at 200 °C (Fig. 6c). No temperature-related changes are observed regarding the elemental distribution of Si, Ti, and O (Fig. 6d–f).

The sample annealed at 300 °C shows larger Ag clusters (approx. 50 to 65 nm) as well as smaller ones with diameters below 10 nm (Fig. 7a). The increased

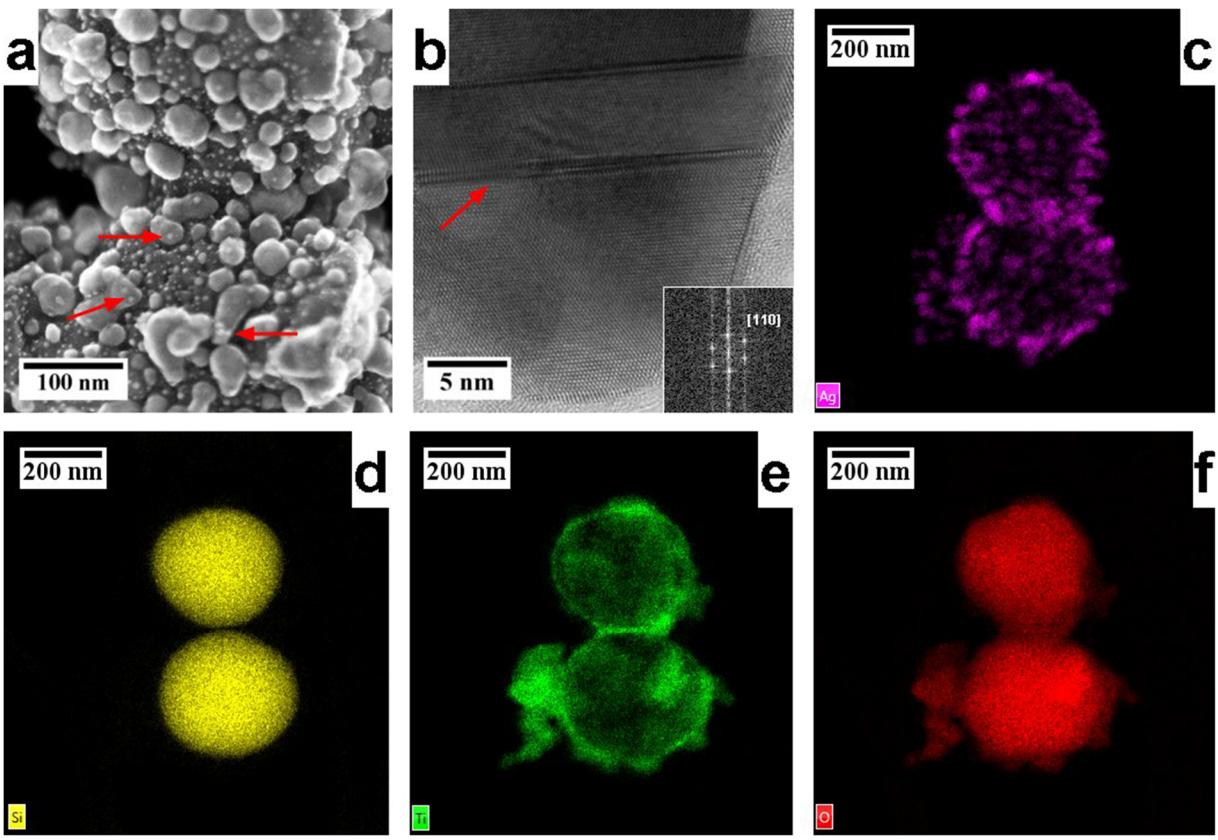

Fig. 6 SiO_2/TiO_2/CR-Ag nanostructures treated at 200 °C obtained via **a** SE and **b** HRTEM. EDS mapping for **c** Ag, **d** Si, **e** Ti, and **f** O

diameter suggests that the applied temperature has likely degraded CR (which was occupying the interstitial sites) thereby disrupting the stability of the CR-Ag nanoparticles and promoting their sintering. Such increase in diameter of the CR-Ag NPs corroborates the blue shift shown and explained previously by UV-Vis spectrometry. The CR-Ag NPs that were deposited on the surface of the second phase of titania sintered at temperatures lower than 300 °C resulting in large (> 100 nm) silver agglomerates observed next to the SiO_2/TiO_2/CR-Ag composites. The measured d-spacing was 2.48 and 2.17 Å which suggested the predominant hexagonal (4H) crystal structure for Ag (inset of Fig. 7b) with corresponding Miller indices of (101) and (1-1$\bar{1}$2). EDS for the sample annealed at 300 °C (Fig. 7c) shows well-defined and dispersed Ag crystals over the SiO_2/TiO_2 surface. Elemental mapping of Si, Ti, Ag, and O (Fig. 8d–f) shows Ag NPs that are free of oxygen (see circled areas and red arrows) suggesting that the composite at 300 °C is chemically stable.

Finally, the SiO_2/TiO_2/CR-Ag structures exposed to 500 °C show Ag particles with diameters that fall in the range of 50 to 120 nm resulting from the agglomeration of silver NPs (Fig. 8a). We can also see an apparent TiO_2 layer that is almost free of silver particles. Here, only a few silver nanocrystals ranging in size from 5 to 15 nm can be seen. However, at a higher magnification (Fig. 8b), dispersed silver NPs ranging in size from 1 to 5 nm are observed on the TiO_2 defects. Such small NPs seem to have resisted the higher temperature indicating the presence of a strong metal-metal oxide interaction. Part of the structure shown in Fig. 8a is free of TiO_2 and Ag NPs on its surface. The explanation here is that Ag NPs were not deposited on the bare SiO_2 surface because TiO_2 was preferred over the SiO_2 surface for nucleation. The literature also indicates that Ag NPs supported on SiO_2 surfaces sinter at temperatures that are much lower than 500 °C (Chen et al. 2011). The d-lattice spacing for this sample estimated to be 2.81 Å, which indicates a Miller index of (200). EDS analyses confirmed that the

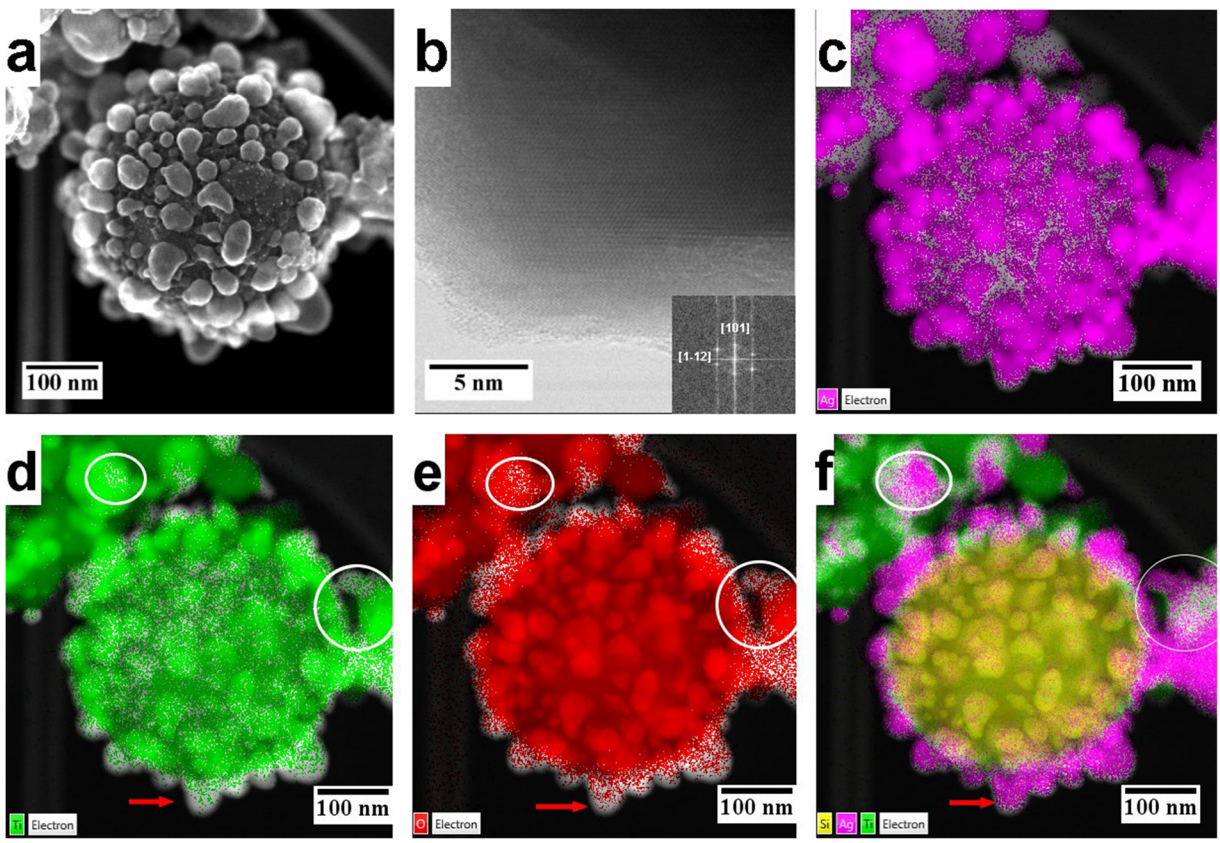

Fig. 7 SiO_2/TiO_2/CR-Ag nanostructures treated at 300 °C obtained via **a** SE and **b** HRTEM. EDS mapping for **c** Ag, **d** Ti, **e** O, and **f** Si, Ti, and Ag

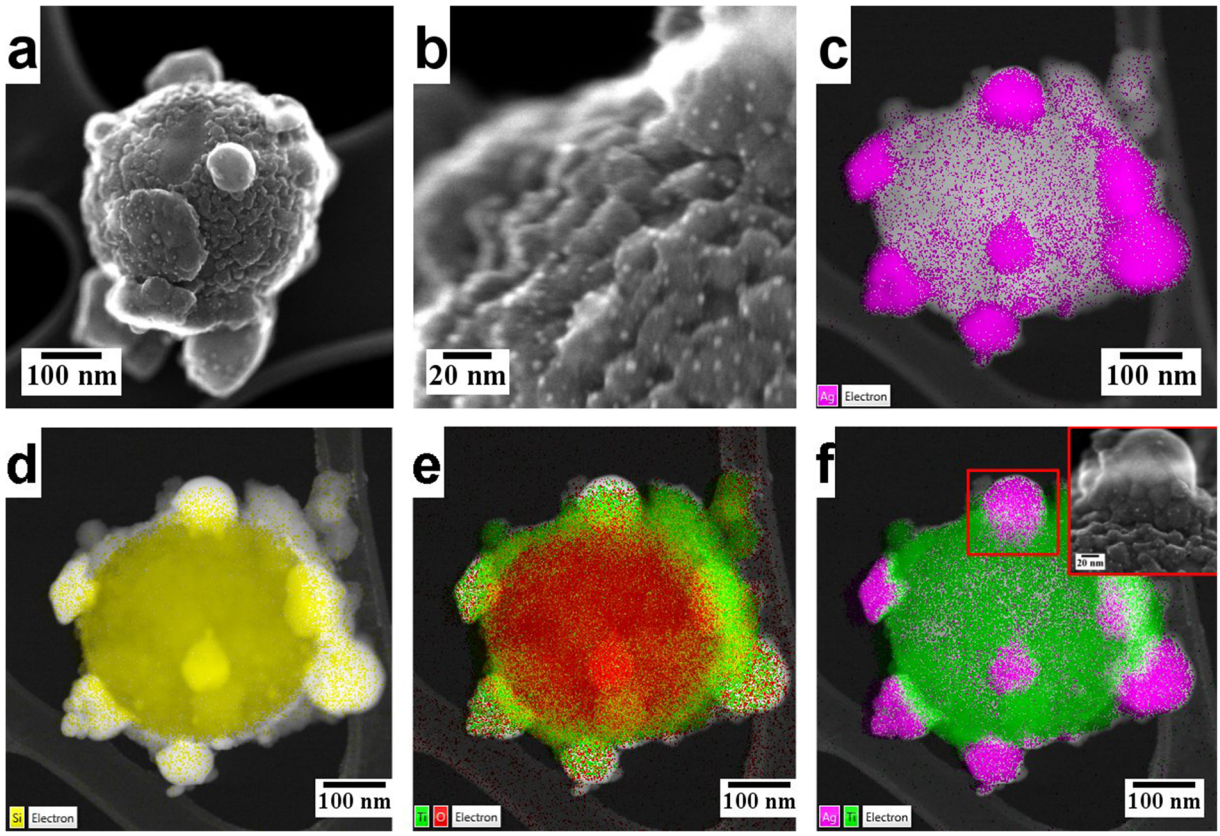

Fig. 8 SiO_2/TiO_2/CR-Ag nanostructures treated at 500 °C obtained via **a** SE and **b** HRTEM. EDS mapping for **c** Ag, **d** Si, **e** Ti and O, and **f** Ti and Ag, *inset* SE of Ag NP embedded in the titania layer

large particles atop the SiO_2/TiO_2 structure were metallic silver (Fig. 8c). The scattering of silver on the entire surface of SiO_2/TiO_2 particles corroborated the existence of silver NPs deposited on TiO_2. SiO_2 particles kept continued to remain stable (Fig. 8d). Same was true for elemental oxygen which occupied the same areas covered by Si and Ti (Fig. 8e). However, in this sample, the large silver particle (enclosed in the rectangle) is embedded in the titania layer (Fig. 8e, f). The growth of the silver crystals affected the stability of the TiO_2 layer, demonstrating strong interactions between the metal NPs and the metal oxide layer. Ag NPs were anchored to TiO_2 film during nucleation and growth; therefore, when Ag NPs grew, the TiO_2 layer became unstable, moving along silver nanoparticle as it kept growing (inset of Fig. 8f).

Crystal growth can occur by different mechanisms. We have described earlier the two most commonly cited ones in the literature, namely PMC and OR. It is difficult to determine which one of the two mechanisms is dominant when it comes to sintering of NPs, particularly for the presence of crystal fringes on the sample without thermal treatment. But based on our observations, PMC process is responsible for the Ag crystal growth. Silver grains in the range of 1 to 5 nm were noted on the surface of large silver particles at all temperatures. This is the effect of the continuous particle migration which allowed us to detect small silver nanoparticle coalescing in the structure of larger ones. We do not attribute such phenomenon to the leaking of CR because, in our analysis, we have always focused the e-beam for a considerable amount of time atop single silver NPs to obtain high-resolution images, and in doing so, we have not observed the formation of any new bumps (Fig. 9).

According to our findings, 300 °C is the maximum temperature that CR-Ag nanoparticles with diameters larger than 10 nm can resist. Higher temperatures cause CR degradation along with the rearrangement of Ag crystal structure. This destabilization incites the migration of silver species to a more stable structure (i.e., larger crystals). As we have seen, crystallites with diameters smaller than 10 nm were detected in all samples including

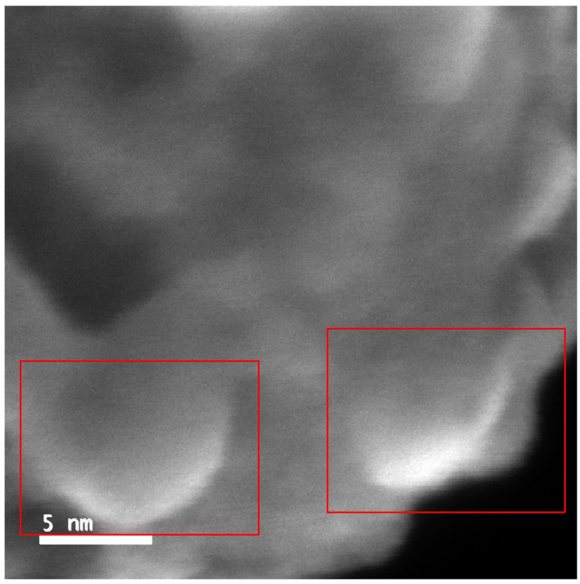

Fig. 9 SiO_2/TiO_2/CR-Ag nanostructures treated at 300 °C. Presence of small Ag grains on the surface of the larger ones

the one annealed at 500 °C. This is due to the structured TiO_2 layer which is inhibiting the surface migration by the strong metal to metal oxide interaction. Such binding energy is higher than the surface free energy of Ag NPs which would otherwise destabilize them.

Conclusions

Methodologies capable of producing thermally stable silver NPs are necessary for future practical applications. In this study, we described how to synthesize novel hybrid structures with thermally stable Ag NPs. The resulting SiO_2/TiO_2/CR-Ag structures are likely to have numerous applications in the fabrication of biosensors, optical devices, catalysts, and integrated circuits due to the presence of chemically selective and thermally stable materials all within one compact structure. The modification of the SiO_2 surface by the construction of the granular titania interfacial layer combined with the active organic-metal nanoparticles deposition generated composites with unique properties, making our experimental design attractive and easily extendable to other metals.

Sintering behavior of CR-Ag NPs was investigated. CR-Ag NPs with larger diameters (10 to 30 nm) showed thermal stability at temperatures as high as 300 °C. Pure metallic Ag NPs with smaller diameters (1 to 5 nm) were observed at temperatures as high as 500 °C with no CR in their structure due to the low melting point of CR. Consequently, two synthesis pathways can be selected depending on the final application of the SiO_2/TiO_2/CR-Ag structures. If the chemical and physical properties of the CR-Ag particles is required, then the synthesis path should be identical to the one described in here. On the other hand, if one wishes to solely exploit the action of thermally stable Ag NPs, then the synthesis path needs to exclude the addition of CR since, without CR, the successful deposition and distribution of Ag NPs relies only on the action of the two stabilizing-reducing agents.

TEM, HRTEM, and SEM data showed the random morphologies and sizes of the CR-Ag as well as well-defined titania coatings at all temperatures. Coalescence of the CR-Ag NPs during the heat treatment was observed. TEM allowed us to identify the potential sintering mechanism (PMC) of the CR-Ag NPs by direct observation of NP coalescing. Close examination of the data shows that PMC sintering process started at temperatures lower than 200 °C when the presence of small particles on the surface of the larger ones was noted. We suggested a slow increase of grain size considering that the temperature was ramped up. The predominant crystal structure was the hexagonal 4H-Ag phase for all the particles analyzed. This was likely a direct outcome of the PMC crystal growth mechanism since particle coalescence facilitated the formation of other crystalline structures that were uncommon in bulk form. EDS analysis showed how the dispersion and relative concentration of silver NPs deposited on the surface of TiO_2 changed as a function of annealing temperature, and furthermore, it validated the stability of the SiO_2/TiO_2 support.

Funding information The authors gratefully acknowledge the financial support of the Consejo Nacional de Ciencia y Tecnología (CONACyT) of the Government of Mexico. The TEM work reported herein was acquired in the Kuiper Materials Imaging and Characterization Facility, supported by NASA (grants #NNX12AL47G and #NNX15AJ22G) and NSF (grant #1531243).

Compliance with ethical standards

Conflict of interest The authors declare that they have no conflict of interest.

References

Abou El-Nour KMM, Eftaiha A, Al-Warthan A, Ammar RAA (2010) Synthesis and applications of silver nanoparticles. Arab J Chem 3:135–140. https://doi.org/10.1016/j.arabjc.2010.04.008

Alford TL, Chen L, Gadre KS (2003) Stability of silver thin films on various underlying layers at elevated temperatures. Thin Solid Films 429:248–254. https://doi.org/10.1016/S0040-6090(03)00034-8

Al-Thabaiti SA, Aazam ES, Khan Z, Bashir O (2016) Aggregation of Congo red with surfactants and Ag-nanoparticles in an aqueous solution. Spectrochim Acta - Part A Mol Biomol Spectrosc 156:28–35. https://doi.org/10.1016/j.saa.2015.11.015

Andrade GFS, Fan MK, Brolo AG (2010) Multilayer silver nanoparticles-modified optical fiber tip for high performance SERS remote sensing. Biosens Bioelectron 25:2270–2275. https://doi.org/10.1016/j.bios.2010.03.007

Aouat Y, Marom G, Avnir D, Gelman V, Shter GE, Grader GS (2013) Organically doped silver nanoparticles deposited on titania nanofibers: enhanced catalytic methanol oxidation. J Phys Chem C 117:22325–22330. https://doi.org/10.1021/jp402663z

Argyle M, Bartholomew C (2015) Heterogeneous catalyst deactivation and regeneration: a review. Catalysts 5:145–269. https://doi.org/10.3390/catal5010145

Cao A, Lu R, Veser G (2010) Stabilizing metal nanoparticles for heterogeneous catalysis. Phys Chem Chem Phys 12:13499–13510. https://doi.org/10.1039/c0cp00729c

Chakraborty I, Carvalho D, Shirodkar SN, Lahiri S, Bhattacharyya S, Banerjee R, Waghmare U, Ayyub P (2011) Novel hexagonal polytypes of silver: growth, characterization and first-principles calculations. J Phys Condens Matter 23:325401–325412. https://doi.org/10.1088/0953-8984/23/32/325401

Chen D, Qu Z, Shen S, Li X, Shi Y, Wang Y, Fu Q, Wu J (2011) Comparative studies of silver based catalysts supported on different supports for the oxidation of formaldehyde. Catal Today 175:338–345. https://doi.org/10.1016/j.cattod.2011.03.059

Chen W, Takai C, Khosroshahi HR, Fuji M, Shirai T (2016) A modified sol–gel method using acetone–ethanol mixed solvent for fast constructing nanometric TiO_2 shells. Ceram Int 42:559–568. https://doi.org/10.1016/j.ceramint.2015.08.146

Costa CAR, Leite CAP, Galembeck F (2003) Size dependence of Stöber silica nanoparticle microchemistry. J Phys Chem B 107:4747–4755. https://doi.org/10.1021/jp027525t

Dai Y, Zou J, Liu D, Niu L, Zhou L, Zhou Y, Zhang X (2018) Preparation of Congo red functionalized Fe_3O_4@SiO_2 nanoparticle and its application for the removal of methylene blue. Colloids Surf A 505:90–98. https://doi.org/10.1016/j.colsurfa.2018.04.033

Dong X-Y, Gao Z-W, Yang K-F, Zhang WQ, Xu LW (2015) Nanosilver as a new generation of silver catalysts in organic transformations for efficient synthesis of fine chemicals. Catal Sci Technol 5:2554–2574. https://doi.org/10.1039/C5CY00285K

Fang ZZ, Wang H (2013) Sintering of ultrafine and nanosized particles. In: Banerjee R, Manna I (eds) Ceramic nanocomposites. Woodhead, Philadelphia, pp 434–469

Hanprasopwattana A, Srinivasan S, Sault AG, Datye AK (1996) Titania coatings on monodisperse silica spheres (characterization using 2-propanol dehydration and TEM). Langmuir 12:3173–3179. https://doi.org/10.1021/la950808a

Hansen TW, Delariva AT, Challa SR, Datye AK (2014) Sintering of nanoparticles: particle migration or Ostwald ripening? Acc Chem Res 46:1720–1730. https://doi.org/10.1021/ar3002427

Henglein A, Giersig M (1999) Formation of colloidal silver nanoparticles: capping action of citrate. J Phys Chem B 103:9533–9539. https://doi.org/10.1021/jp9925334

Kopangkhotso H, Singh M, Singhal S (2015) Effects of size and shape on thermodynamic properties of nanomaterials. J Thermodyn 2013:1–5. https://doi.org/10.1155/2013/328051

Lee HB, Yoo YM, Han YH (2006) Characteristic optical properties and synthesis of gold-silica core-shell colloids. Scr Mater 55:1127–1129. https://doi.org/10.1016/j.scriptamat.2006.08.044

Luo W, Hu W, Xiao S (2008) Size effect on the thermodynamic properties of silver nanoparticles. J Phys Chem C 112:2359–2369. https://doi.org/10.1021/jp0770155

Maldonado C, Fierro JLG, Birke G et al (2010) Conversion of methanol to formaldehyde on TiO_2 supported Ag nanoparticles. J Chil Chem Soc 55:506–510. https://doi.org/10.4067/S0717-97072010000400021

Moon K-S, Dong H, Maric R, Pothukuchi S, Hunt A, Li Y, Wong CP (2005) Thermal behavior of silver nanoparticles for low-temperature interconnect applications. J Electron Mater 34:168–175. https://doi.org/10.1007/s11664-005-0229-8

Moulijn JA, Van Diepen AE, Kapteijn F (2001) Catalyst deactivation: is it predictable? What to do? Appl Catal A Gen 212:3–16. https://doi.org/10.1016/S0926-860X(00)00842-5

Pham X-H, Lee M, Shim S, Jeong S, Kim HM, Hahm E, Lee SH, Lee YS, Jeong DH, Jun BH (2017) Highly sensitive and reliable SERS probes based on nanogap control of a Au–Ag alloy on silica nanoparticles. RSC Adv 7:7015–7021. https://doi.org/10.1039/C6RA26213A

Safaei A, Attarian Shandiz M (2009) Size-dependent thermal stability and the smallest nanocrystal. Phys E Low-Dimensional Syst Nanostructures 41:359–364. https://doi.org/10.1016/j.physe.2008.07.023

Shter GE, Behar-Levy H, Gelman V, Grader GS, Avnir D (2007) Organically doped metals—a new approach to metal catalysis: enhanced Ag-catalyzed oxidation of methanol. Adv Funct Mater 17:913–918. https://doi.org/10.1002/adfm.200600482

Stöber W, Fink A, Bohn E (1968) Controlled growth of monodisperse silica spheres in the micron size range. J Colloid Interface Sci 26:62–69. https://doi.org/10.1016/0021-9797(68)90272-5

Su Y, Shi B, Liao S, Zhao J, Chen L, Zhao S (2016) Silver nanoparticles/N-doped carbon-dots nanocomposites derived from Siraitia Grosvenorii and its logic gate and surface-enhanced Raman scattering characteristics. ACS Sustain Chem Eng 4:1728–1735. https://doi.org/10.1021/acssuschemeng.5b01698

Volkman SK, Yin S, Bakhishev T, Puntambekar K, Subramanian V, Toney MF (2011) Mechanistic studies on sintering of silver nanoparticles. Chem Mater 23:4634–4640. https://doi.org/10.1021/cm202561u

Wallace WT, Min BK, Goodman DW (2005) The stabilization of supported gold clusters by surface defects. J Mol Catal A Chem 228:3–10. https://doi.org/10.1016/j.molcata.2004.09.085

Wang Y, Chen L, Ping L (2012) Biocompatible triplex Ag@SiO_2@mTiO_2 core-shell nanoparticles for simultaneous fluorescence-SERS bimodal imaging and drug delivery. Chem Eur J 18:5935–5943. https://doi.org/10.1002/chem.201103571

Yan W, Mahurin SM, Pan Z, Overbury SH, Dai S (2005) Ultrastable Au nanocatalyst supported on surface-modified TiO_2 nanocrystals. J Am Chem Soc 127:10480–10481. https://doi.org/10.1021/ja053191k

Ye X, Cai S, Zheng C, Xiao X, Hua N, Huang Y (2015) SiO_2/TiO_2/Ag multilayered microspheres: preparation, characterization, and enhanced infrared radiation property. Appl Surf Sci 345: 279–285. https://doi.org/10.1016/j.apsusc.2015.03.098

Yosef I, Avnir D (2011) Entrapment of dye molecules within submicron silver particles. J Nanopart Res 13:3929–3937. https://doi.org/10.1007/s11051-011-0315-1

Yu J-G, Yu H-G, Cheng B, Zhao XJ, Yu JC, Ho WK (2003) The effect of calcination temperature on the surface microstructure and photocatalytic activity of TiO_2 thin films prepared by liquid phase deposition. J Phys Chem B 107:13871–13879. https://doi.org/10.1021/jp036158y

Zhang J, Li Y, Zhang Y, Chen M, Wang L, Zhang C, He H (2015) Effect of support on the activity of Ag-based catalysts for formaldehyde oxidation. Sci Rep 5:12950–12960. https://doi.org/10.1038/srep12950

Zhou Z-Y, Tian N, Li J-T, Broadwell I, Sun SG (2011) Nanomaterials of high surface energy with exceptional properties in catalysis and energy storage. Chem Soc Rev 40: 4167–4185. https://doi.org/10.1039/c0cs00176g